The International Journal of Advanced Manufacturing Technology
https://doi.org/10.1007/s00170-022-08954-2

ORIGINAL ARTICLE

Novel design concept for shrink-fitted bimetallic sleeve roll in hot rolling mill

Rahimah Abdul Rafar[1] · Nao-Aki Noda[1] · Hiroyuki Tsurumaru[1] · Yoshikazu Sano[1] · Yasushi Takase[1]

Received: 24 September 2021 / Accepted: 18 February 2022

Abstract
The rolls are classified into two types; one is a single-solid type roll, and the other is a shrink-fitted assembled type sleeve roll consisting of a sleeve and a shaft. The sleeve roll is successfully used as a large back-up roll used in rolling. However, sometimes, the interfacial slip appears although the slippage resistance torque T_r is designed to be larger than the motor torque. In this paper, the FEM simulation is performed to clarify the phenomena in real rolling. It is found that the interfacial slip is accelerated significantly with increasing the motor torque. The circumferential slippage under zero torque can be explained from the non-uniform deformation due to the rolling force P. This is because the displacement increase rate increases with increasing the force P. Finally, a novel design concept is proposed for sleeve rolls from the present discussion.

Keywords Bimetallic work roll · Rolling roll · Shrink-fitted · Interfacial slip · Motor torque · Sleeve

1 Introduction

In steel manufacturing industries, rolling processes more tonnage than any other metalworking process [1–15]. Four-high type consisting of a pair of work rolls and a pair of back-up rolls are most commonly used as strip mills. The technical innovations in the rolling strip mills have been conducted on the application and the improvement of large sleeved back-up roll [1–3], rolled steel with cross-section [4, 5], hot rolling strip mills [6–9], and bimetallic work roll [10–15].

Figure 1a illustrates the rolling roll in steel roughing of a hot rolling stand mill. The rolls can be classified into two types; one is a single-solid type, and the other is a shrink-fitted assembly type consisting of a sleeve and a shaft as shown in Fig. 1b, c. The shrink-fitted assembly type rolls are efficiently used as the back-up rolls having large trunk diameter exceeding 1000 mm and used for large H-section steel rolling rolls [1–3]. Those sleeve rolls have several advantages; the shaft can be reused by replacing the damaged sleeve due to the abrasion and the surface roughening and the sleeve wear resistance can be improved independently without loosening the shaft ductility.

On the other hand, this shrink-fitted assembly type roll has several particular problems such as residual bending of the roll, fatigue fracture at the end of the sleeve, and sleeve fracture due to the circumferential slippage [5–12]. Among them, there is no detailed studies are available for the interfacial slippage in a rolling roll. It should also be pointed out that the interfacial slippage in shrink-fitted roll sometimes occurs even if the resistance torque at the interface is larger than the motor torque. Considering no quantitative study available for rolling rolls, by focusing on the sleeve displacement, the previous study assumed a rigid shaft modeling to simplify the phenomenon and to realize the slippage in the numerical simulation [13].

Although few studies are available for this new failure in shrink-fitted assembly type rolls, a similar phenomenon is known as "interfacial creep" in ball bearing appearing between the bearing and the stationary shaft and between the bearing and the housing [16–26]. However, even in the ball bearing field, few papers discussed the phenomenon quantitatively. In our previous study, therefore, the interfacial slip in the shrink-fitted roll under the free rolling condition was discussed without considering motor torque [14]. Then, it was found that the interfacial slip occurs even under free rolling conditions and under no friction and no motor torque. However, in the real rolling process, to reduce the thickness

✉ Nao-Aki Noda
noda.naoaki844@mail.kyutech.jp

[1] Mechanical Engineering Department, Kyushu Institute of Technology, 1-1 Sensuicho, Tobata, Kitakyushu 804-8550, Japan

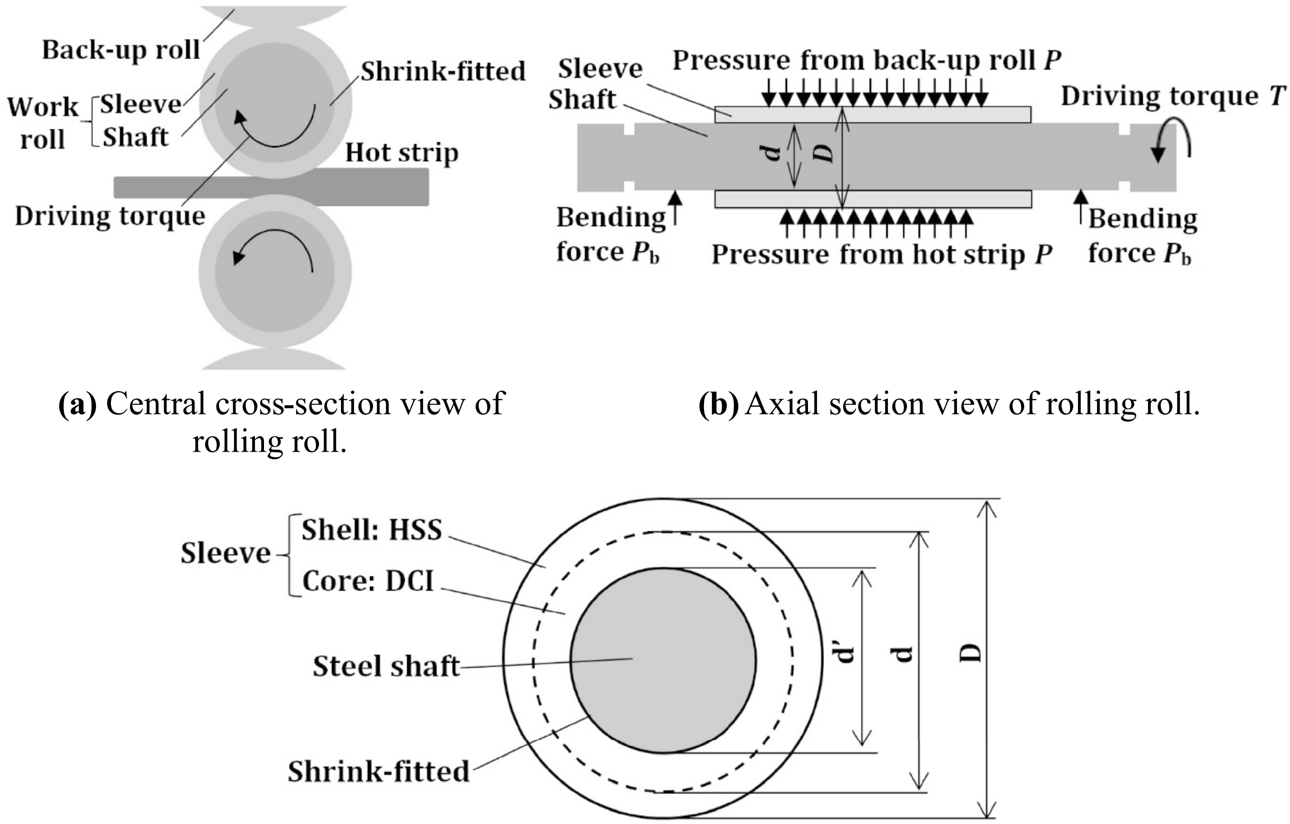

(a) Central cross-section view of rolling roll.

(b) Axial section view of rolling roll.

(c) A target of this study: HSS bimetallic roll in central cross-section.

Fig. 1 Schematic illustration for real hot strip rolling roll

of the rolling plate, a pair of sleeve rolls is driven by motor torque. Far differently from free rolling, a larger amount of slippage may happen due to the motor torque.

To clarify the effect of the motor torque on the interfacial slip, in this study, the actual work roll of a hot rolling stand mill will be simulated under a similar condition of the real roll. Figure 1a illustrates that the motor torque and the balanced frictional force from the rolled steel promote the slippage significantly. In the actual work, roll of a hot rolling stand, differently from ball bearings, such promoted slippage may cause a serious failure. In this sense, the effects of the shrink-fitting ratio and the friction coefficient will be discussed since they may contribute to slippage resistance. Finally, the novel design concept for the sleeve roll will be proposed from the discussion.

2 Simulation for non-uniform slip versus overall slip considered in conventional design

Figure 1 shows a sleeve assembly type roll used in rolling roll. Figure 1a shows the central cross-section and Fig. 1b shows the axial cross-section. As shown in Fig. 1, the sleeve roll consists of a shrink-fitted sleeve and shaft. Figure 1c shows an example of a commonly used bimetallic sleeve roll made by the centrifugal casting method. Here, the outer layer is high-speed steel (HSS) having high abrasion resistance and the inner layer is ductile casting iron (DCI) having high ductility. To simplify the analysis and to clarify "the interfacial slip," this present study will focus on a single material sleeve roll instead of the bimetallic sleeve roll. In the field of ball bearing, the phenomenon of such slip is referred to as "interfacial creep." In this paper, however, the phenomenon is named "an interface slip" according to the usage of sleeve assembly type rolls in the rolling field.

As shown in Fig. 1a, the roll is subjected to the contact force P from the back-up roll, the rolling force P_h, and the frictional force S (shear force) from the rolling plate. Since two-dimensional modeling is used in this study, the external force per unit length, as well as motor torque T, should be considered. In Fig. 1b, the back-up roll is longer than the width of the rolling plate; and therefore, the bending force P_b is acting at the bearing. Here, the rolling force P, the rolling reaction force P_h, and the bending force P_b should be balanced, but P_b is estimated to be less than 10% of P and P_h [5]. Therefore, in this study, by assuming the bending force

$P_b = 0$, the rolling force ($= \sim P \times$ back-up roll body length) is equal to the rolling force ($= \sim P_h \times$ strip width) as $P \simeq P_h$. This modeling refers to the loading at the fifth stage of the hot finishing roll [5].

Figure 2 indicates the numerical simulation model used in this study concerning the actual roll approach. The rotation of the roll is expressed by the circumferential load transfer on the roll surface without rotating the roll [13, 14]. Figure 2a shows two-dimensional real roll conditions. Figure 2b shows a roll model in which the entire shaft is rigid assumed in the previous paper to simplify the phenomenon and to realize the slippage in the numerical simulation [13]. This is because this phenomenon is hard to be proved and considering no quantitative study available for rolling rolls. Based on the analysis of the rigid shaft, the analysis method can be confirmed and clarified for the elastic shaft, which is closer to the real roll conditions. As shown in Fig. 2c, to restrain the displacement and rotation of the center of the roll in order to justify the elastic deformation of the sleeve and shaft, a small rigid body at the center of the shaft is introduced. In this analysis, the rigid body size at the center has been confirmed does not affect the result and the diameter is set to be 8 mm. The load transfer interval is set to be $\varphi = 4^o$ in consideration of computational time without loosening the analysis accuracy.

The roll is subjected to the force P from the back-up roll, the rolling reaction force P, and the frictional force S from the roll material, and the driving torque T from the motor. In the previous paper, the interface slip was discussed under the motor torque $T = 0$ and the friction force $S = 0$ [14]. In this paper, the interfacial slip will be considered under driving torque $T \neq 0$ and the friction force $S \neq 0$.

To distinguish from "an overall slip" considered in the conventional design, the slip considered in this study can be named as "a non-uniform slip." This is because due to the applied force P, a non-uniform deformation appears at the interface. Instead, the conventional machine design has considered the following condition conventionally stating that the motor torque should be smaller than the slippage resistance torque T_r as defined in Eq. (1).

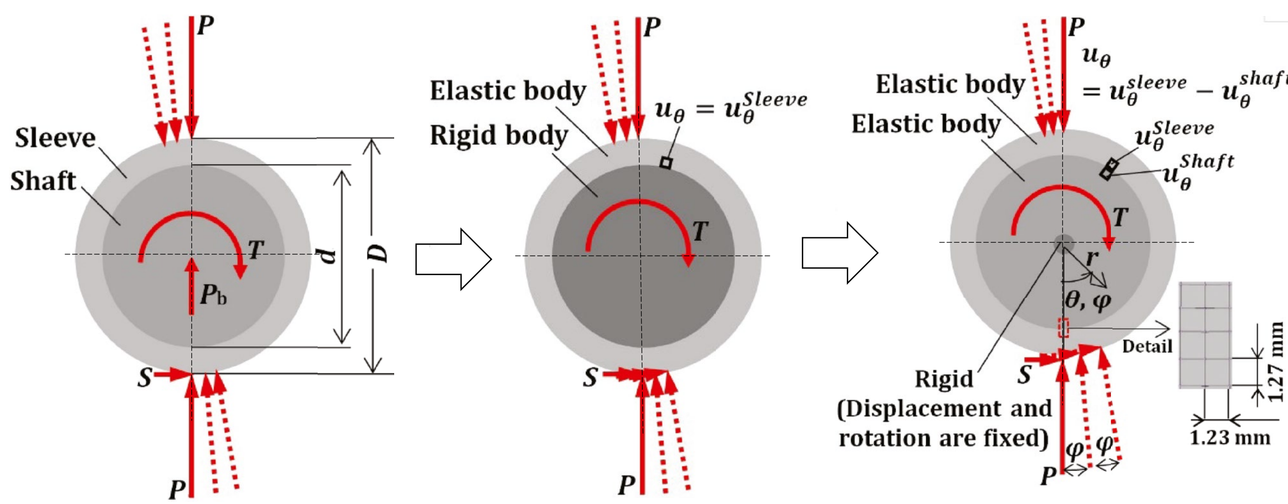

P: Load form back-up roll and hot strip (N)
S: Frictional force (N)
P_b: Bending force from bearing (N)
T: Driving torque (Nm), $T = SD/2$
T_m: Rated torque of motor (Nm)
T_r: Slippage resistance torque (Nm)

(a) Real roll

$T = 0 \sim 10T_m$
$10T_m > T_r = 3193$ Nm /mm
$T_m = 471$ Nm /mm
$P_b = 0$

(b) Rigid shaft when $E_{shaft} \to \infty$

θ : Circumferential angle of sleeve
φ_0: Load shift interval
φ : Load shift angle

(c) Elastic shaft when $E_{shaft} =$ 210 GPa

Fig. 2 Modeling for "non-uniform interfacial slip" different from "overall slip" considered in the conventional design

$$T < T_r, T_r = \xi \frac{d}{2} \pi d l_b \mu \sigma_{r_{\mathrm{shrink}}} (Nm/mm) \tag{1}$$

Here, d is the shaft outer diameter, which is equal to the sleeve inner diameter, l_b is the roll barrel length, μ is the friction coefficient between the shaft and the sleeve, and $\sigma_{r_{shrink}}$ is the shrink-fitting stress. The notation ξ denotes the effective shrink-fitting ratio considering manufacturing error. Although under $T < T_r$ the overall slip can be prevented, the non-uniform slip may happen.

The sleeve resistance torque T_r can be calculated as $T_r = 3193$ Nm/mm under the standard conditions when $\xi = 1$, $l_b = 1$ mm, $\mu = 0.3$, $\sigma_{r_{shrink}} = -21.6$ MPa, and $\delta/d = 0.5 \times 10^{-3}$. The real torque can be expressed as $T_m = \eta 471$ Nm/mm by using the reduction ratio $\eta = 1.882$ [39]. In this study, $\eta = 1$ is used to express the rated motor torque as $T_m = 471$ Nm/mm to confirm that the smaller rated torque may cause the interfacial slip.

In the shrink-fitting type roll, the slippage resistance torque T_r on the roll side has to be larger than the shaft driving torque T as shown in Eq. (2) by using α denoting the slippage safety factor.

$$T_r = \alpha T (Nm/mm) \tag{2}$$

Under the rated motor torque as $T = T_m = 471$ Nm/mm, the safety factor $\alpha = 6.77$ from Eq. (2). The shear force S can be obtained from Eq. (3).

$$T_m = S \frac{D}{2} (Nm/mm) \tag{3}$$

When the rated motor torque is $T_m = 471$ Nm/mm, the friction force (=shearing force) is obtained as $S = 1346$ Nm/mm from Eq. (3).

On the basis of the experience and skills for engineering applications, the finite element method (FEM) should be well conducted to realize the interface slippage. Therefore, Fig. 2c also shows the mesh division for the finite element simulation model. In the previous studies, the FEM mesh error was discussed for bonded problems and the mesh-independent technique was proposed confirming that the provided displacement boundary condition is relatively insensitive to mesh division [27–30]. The tightening process of the pitch-difference nut with the dynamic deformation was investigated through consecutive quasi-static analyses to clarify the contact status change in the bolt and nuts threads [31, 32]. On the basis of those skills, the axial movement of the shaft during the ceramic roll rotation was analyzed by shifting the load on the fixed shaft [33–36]. The circumferential sleeve slippage will be realized in this study by extending the above technique to the elastic contact quasi-static analysis for rolling rolls and applying FEM code Marc/Mentat 2012. In this code, the complete Newton–Raphson method and the direct constraint method for the contact analysis are used. As shown in Fig. 2c, 4-node quadrilateral plane strain elements are used with the number of mesh elements are 309,440 with confirming the mesh independence of the results [37].

Table 1 shows the mechanical properties, dimensions, and boundary conditions of the model in Fig. 2c. In this study, the loading condition used is based on the data at no. 5 stand for roll hot strip finishing roll mill [4, 5]. Assume the concentrated load $P = P_0 = 13270$ N/mm from the back-up roll, which is equal to the reaction from the strip [4, 5]. By replacing Hertzian contact stress with the concentrated force P, the small effect on the analysis can be confirmed. The shrink-fitting ratio is defined as δ/d, where δ is the diameter difference between sleeve inner diameter and shaft outer diameter. Usually, the shrink-fitting ratio in the range $\delta/d = 0.4 \times 10^{-3} \sim 1.0 \times 10^{-3}$ is applied to sleeve rolls based on the long year experience. This is because a smaller value $\delta/d < 0.4 \times 10^{-3}$ may cause an interface to slip easily and a larger value $\delta/d < 0.4 \times 10^{-3}$ may increase the risk of sleeve fracture [6]. In this paper, $\delta/d = 0.5 \times 10^{-3}$ is focused to study the irreversible interfacial slip. The effect of the shrink-fitting ratio is discussed in Sect. 4.2. Previously, regarding the friction coefficient μ which controls the slippage resistance on the interface, $\mu = 0.2$ was used in an experimental study, and $\mu = 0.4$ was often used for steel surfaces [1, 38]. Therefore, since $\mu = 0.2 \sim 0.4$ is usually used for sleeve assembly type rolls, the friction coefficient $\mu = 0.3$ between the sleeve and the shaft is used in this study.

The relative displacement accumulation between the sleeve and shaft may represent the interfacial slip. In Fig. 3a, the relative displacement between the sleeve and shaft due to the load shifting $P(0) \sim P(\varphi)$ when the load moves from the angle $\varphi = 0$ to $\varphi = \varphi$ is defined as $u_\theta^{P(0)\sim P(\varphi)}(\theta, \varphi)$. The relative displacement u_θ between the elastic shaft and elastic sleeve on the shrink-fitted surface can be expressed as in Eq. (4) which is defined as the interfacial slip on the shrink-fitted surface.

$$u_\theta^{P(0)\sim P(\varphi)}(\theta, \varphi) = u_{\theta,Sleeve}^{P(0)\sim P(\varphi)}(\theta, \varphi) - u_{\theta,Shaft}^{P(0)\sim P(\varphi)}(\theta, \varphi) \tag{4}$$

Here, notation φ denotes the angle where the load is shifting and notation θ denotes the position where the displacement is evaluated. The load $P(\varphi)$ used in this study is defined as the symmetry forces acting at $\varphi = \varphi$ and $\varphi = \varphi + \pi$. The relative displacement $u_\theta(\theta, \varphi)$ at $\theta = \theta$ when the pair of loads are applied at $\varphi = 0$ to $\varphi = \varphi$ and $\varphi = \pi$ to $\varphi = \varphi + \pi$ is denoted as $u_\theta^{P(0)\sim P(\varphi)}(\theta, \varphi)$. To express the amount of the slip with increasing φ, the average displacement can be defined in the following equation:

$$u_{\theta,ave.,T=T_m}^{P(0)\sim P(\varphi)}(\varphi) = \frac{1}{2\pi} \int_0^{2\pi} u_\theta^{P(0)\sim P(\varphi)}(\theta, \varphi) d\theta \tag{5}$$

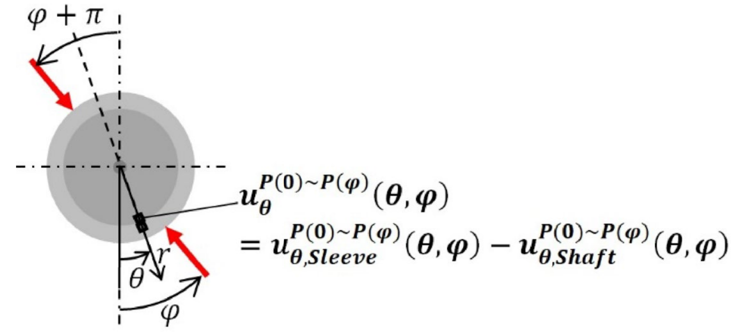

$$u_{\theta,ave.,T=T_m}^{P(0)\sim P(\varphi)}(\varphi) = \frac{1}{2\pi}\int_0^{2\pi} u_{\theta}^{P(0)\sim P(\varphi)}(\theta, \varphi)\, d\theta$$

(a) Definition of interfacial displacement $u_{\theta}^{P(0)\sim P(\varphi)}(\theta, \varphi)$ due to the load shifting $P(0)\sim P(\varphi)$.

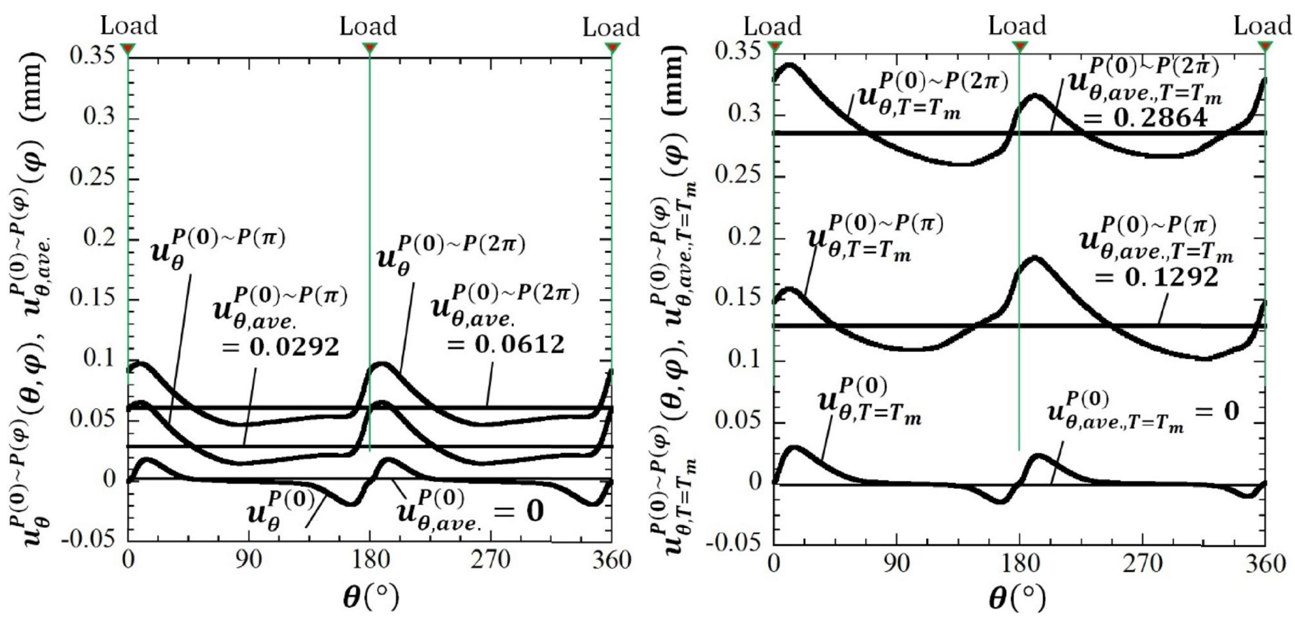

(b) Non-uniform interfacial slip for $T = 0$. **(c)** Non-uniform interfacial slip for $T = T_m$.

Fig. 3 (**a**) Definition of $u_{\theta}^{P(0)\sim P(\varphi)}$, (**b**) $u_{\theta}^{P(0)\sim P(\varphi)}$ when $T = 0$ and $E_{\text{shaft}} = 210$ GPa, and (**c**) $u_{\theta}^{P(0)\sim P(\varphi)}$ when $T = T_m$ and $E_{\text{shaft}} = 210$ GPa

Figure 3b shows the effect of no torque condition $T = 0$ on the displacement distribution $u_{\theta}^{P(0)\sim P(\varphi)}(\theta, \varphi)$ and Fig. 3c shows the effect of the rated motor torque $T = T_m$ on the displacement distribution $u_{\theta}^{P(0)\sim P(\varphi)}(\theta, \varphi)$ when the load is moving to $\varphi = 0$, $\varphi = \pi$ and $\varphi = 2\pi$. As shown in Fig. 3b, the average displacement is zero as $u_{\theta,ave.}^{P(0)}(\varphi) = 0$ when the initial load P is applied at $\varphi = 0$. It is important to note that the distribution of the displacements $u_{\theta}^{P(0)}(\theta)$ is non-zero except at $\theta = 0$, π, and 2π. This non-zero displacement means such local slippage may appear once the load is applied. Although $u_{\theta}^{P(0)}(\theta)$ is symmetric as shown in Fig. 3b, with increasing the load shifting angle φ, the average displacement $u_{\theta,ave.}^{P(0)\sim P(\varphi)}(\varphi)$ increases after losing the symmetry. On the other hand, as shown in Fig. 3c, at the initial load $\varphi = 0^o$, the magnitude of the displacement is different near both sides of the load position (at $\theta < 0$ and $\theta > 0$) on which the shear forces are applied

Table 1 Mechanical properties, dimensions, and boundary conditions in Fig. 2c [13, 14]

Mechanical properties	Sleeve	Young's modulus of steel sleeve E_{sleeve}	210 GPa
		Poisson's ratio of steel sleeve υ	0.28
	Shaft	Young's modulus of elastic shaft E_{shaft}	210 GPa
		Poisson's ratio of steel shaft υ	0.28
Roll size		Outer diameter of sleeve	700 mm
		Inner diameter sleeve d	560 mm
Shrink fitting		Shrink fitting ratio δ/d	0.5×10^{-3}
		Friction coefficient between sleeve and shaft μ	0.3
External force		Concentrated load per unit thickness $P = P_0$	13,270 N/mm Total: 1.327×10^{7} N Rolled width: 1000 mm
		Frictional force per unit thickness S	1346 N/mm
		Rated torque of motor per unit thickness T_m	471 Nm/mm
		Resistance torque per unit thickness T_r	3193 Nm/mm
		Bending force from bearing P_b	0 N/mm

($\theta = 0^o$). Due to the shear force, the magnitude of the displacement is larger on the positive direction of the shear force ($\theta > 0^o$) and $\left|u_{\theta,T=T_m}^{P(\varphi)}(-\theta)\right| < \left|u_{\theta,T=T_m}^{P(\varphi)}(+\theta)\right|$. Moreover, the displacement distributions are not symmetric anymore due to the effect of the rated motor torque T_{m} as given in the following equation:

$$\left|u_{\theta,T=T_m}^{P(\varphi)}(-\theta)\right| < \left|u_{\theta,T=T_m}^{P(\varphi)}(+\theta)\right| \tag{6}$$

As shown in Fig. 3b, c, the average displacement of half roll rotation $u_{\theta,ave.}^{P(0)\sim P(\pi)}(\varphi)$ when $T = T_m$ is about 4 times larger than that under no torque condition $T = 0$. In addition, the average displacement of one roll rotation $u_{\theta,ave.}^{P(0)\sim P(2\pi)}(\varphi)$ when $T = T_m$ is about 5 times larger than no torque condition $T = 0$. This result shows that the presence of the motor torque significantly accelerates the interfacial slip.

3 Interfacial slip under rated motor torque $T = T_m$

3.1 Interfacial displacement and increase rate of interfacial displacement

Figure 4a shows the relationship between the average displacement $u_{\theta,\text{ave.}}^{P(0)\sim P(\varphi)}(\varphi)$ and the load rotation angle φ for the elastic shaft under no toque $T = 0$ and under the rated motor torque $T = T_m$. In Fig. 4a, regardless of the motor torque condition, the average value increases almost linearly during the initial roll rotation. The average displacement of one roll rotation $u_{\theta,ave.}^{P(0)\sim P(2\pi)}(\varphi)$ when $T = T_m$ is about 5 times larger than that under no torque condition $T = 0$. From Fig. 4a, it should be noted that the average displacement $u_{\theta,\text{ave.}}^{P(0)\sim P(\varphi)}(\varphi)$ at $\varphi = 2\pi \times 2$, that is, 2 roll rotations, is about 2 times larger than $u_{\theta,\text{ave.}}^{P(0)\sim P(\varphi)}(\varphi)$ at $\varphi = 2\pi$. Therefore, the slippage increases linearly after the initial roll rotation $\varphi \geq 2\pi$.

Therefore, as shown in Fig. 4b, the interfacial slip is quantitatively evaluated by focusing on the increase rate of interfacial displacement $\mathrm{d}u_\theta^{P(0)\sim P(2\pi)}(\theta, \varphi)/\mathrm{d}\varphi$. In Fig. 4b, the displacement increase rate $\mathrm{d}u_\theta^{P(0)\sim P(2\pi)}(\theta, \varphi)/\mathrm{d}\varphi$ under the rated motor torque $T = T_m$ is nearly 5 times larger than under no toque condition $T = 0$. In addition, regardless of the motor torque condition, before the initial one roll rotation, the interfacial slip is unstable since the displacement increase rate $\mathrm{d}u_\theta^{P(0)\sim P(\varphi)}(\theta, \varphi)/\mathrm{d}\varphi\Big|_{\varphi<360^\circ}$ increases gradually. After the initial one roll rotation, however, the interfacial slip becomes stable since $\mathrm{d}u_\theta^{P(0)\sim P(\varphi)}(\theta, \varphi)/\mathrm{d}\varphi\Big|_{\varphi\geq360^\circ}$ is constant. The displacement increase rate $\mathrm{d}u_\theta^{P(0)\sim P(\varphi)}(\theta, \varphi)/\mathrm{d}\varphi$ for more than one roll rotation can be evaluated accurately from the displacement increase rate $\mathrm{d}u_\theta^{P(0)\sim P(\varphi)}(\theta, \varphi)/\mathrm{d}\varphi\Big|_{\varphi=360^\circ}$ at the initial one roll rotation.

3.2 Slippage zone affected by the motor torque

Figure 5 shows the shear stress distribution $\tau_{r\theta}^{P(0)\sim P(2\pi)}$ in comparison with the frictional stress $\mu\sigma_r^{P(0)\sim P(2\pi)}$ along the shrink-fitting surface. Figure 5a shows the result of $E_{shaft} = 210$ GPa after the initial one roll rotation $P(0) \sim P(2\pi)$ under free rolling roll condition $T = 0$. Figure 5b shows the result of $E_{shaft} = 210$ GPa after the initial one roll rotation $P(0) \sim P(2\pi)$ under rated motor torque $T = T_m$. The notation $P(0) \sim P(2\pi)$ denotes the initial one roll rotation expressed by the load shifting on the fixed roll from $\varphi = 0$ to $\varphi = 2\pi$. Although the displacement increases with increasing φ as shown in Fig. 4a, the preceding paper confirmed that the stress σ_θ change slightly with less than 8% by increasing φ [15]. It has been

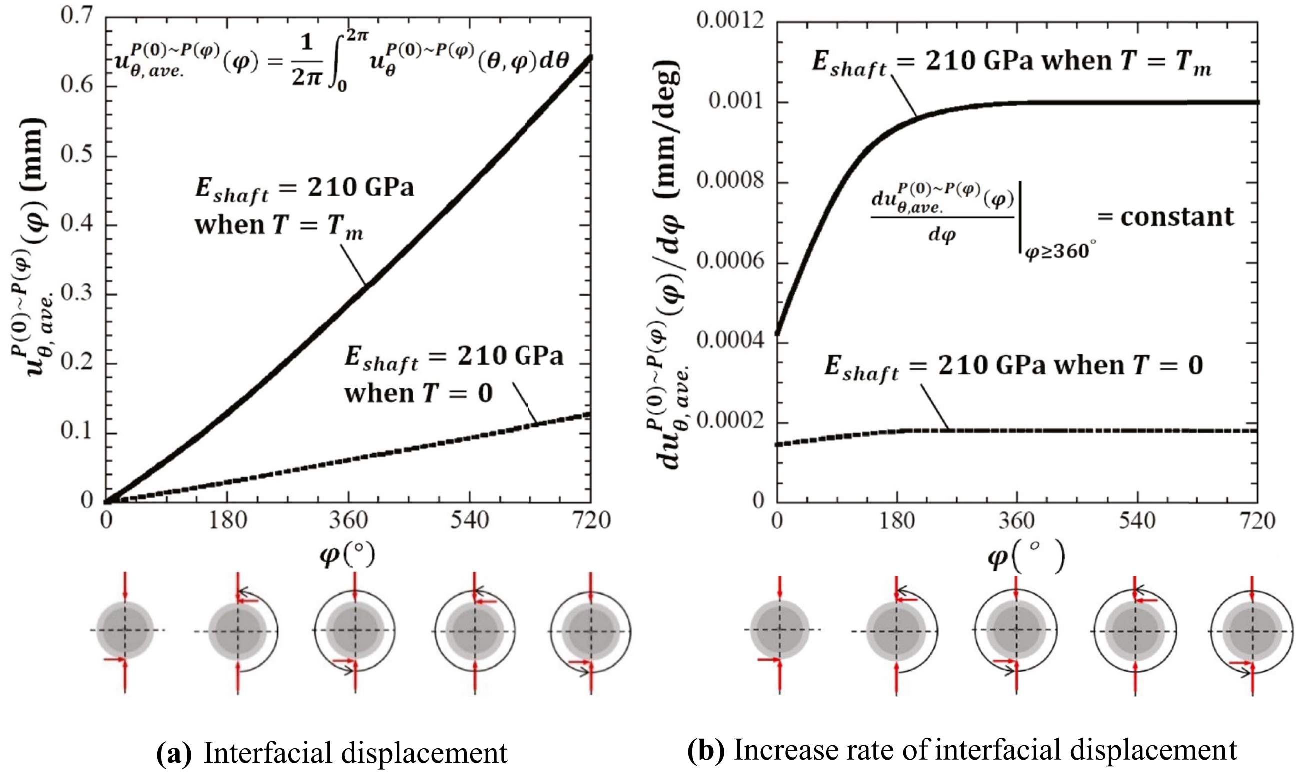

Fig. 4 Interfacial displacement and increase rate of interfacial displacement for elastic shaft E_{shaft} = 210 GPa when T = 0 and $T = T_m$

confirmed that the slippage zone does not change after one rotation of the load.

In the previous experimental studies for sleeve roll [1], the friction coefficient $\mu = 0.2$ was used in an experimental study to discuss the slippage resistance on the interface. For the steel surfaces in general, $\mu = 0.4$ was often used [38]. Therefore, in this study, the friction coefficient $\mu = 0.3$ is assumed between the sleeve and the shaft. By considering the FEM accuracy, the irreversible relative displacement may appear when $\tau_{r\theta} \cong |\mu\sigma_r|$ within the error $\pm$ 1 MPa. This region is defined as the slippage zone ℓ_{slip}. In the previous paper [12], the slippage zone ℓ_{slip} was named "quasi-equilibrium stress zone $\tau_{r\theta} \cong |\mu\sigma_r|$." As shown in Fig. 5, the slippage zone ℓ_{slip} is much larger under rated motor torque $T = T_m$ (Fig. 5b) compared with under the free rolling $T = 0$ (Fig. 5a). This is the reason why the interfacial displacement increases in Fig. 4a due to the rated motor torque $T = T_m$.

4 Effects of design factors and new design concept based on non-uniform slip

4.1 Effect of motor torque *T* on non-uniform slip

In the above discussion, the rated motor torque T_m has been applied to the roll. In addition to the rated motor torque T_m, sometimes, excessively large torque is applied to the shaft of the real roll. This is because even though the roll is driven by a rated motor, several factors affect larger torque such as reduction ratio η, upper and lower roll distribution ratio, over torque, and impact coefficient when the rolled material is caught. Therefore, in this study, in addition to the no torque condition $T = 0$ and the rated motor torque $T = T_m$, other torque conditions $T = 2T_m$, $T = 3T_m$ are also applied.

Figure 6a shows the effect of torque T normalized by the reference value T/T_m on the average displacement $u_{\theta,ave.T}^{P(0)\sim P(2\pi)}(\varphi)$ under one roll rotation $\varphi = 2\pi$ when the load $P = P_0$ for the elastic shaft E_{shaft} = 210 GPa as well as rigid shaft $E_{shaft} = \infty$. With increasing T/T_m and $u_{\theta,ave.T}^{P(0)\sim P(2\pi)}(\varphi)$ increases significantly. The average displacement $u_{\theta,ave.T}^{P(0)\sim P(2\pi)}(\varphi)$ under the rated motor torque $T = T_m$ for the elastic shaft is 4 times larger than that of the rigid shaft, and $u_{\theta,ave.T}^{P(0)\sim P(2\pi)}(\varphi)$ under $T = 3T_m$ for the elastic shaft is 9 times larger than the rigid shaft. As shown in Fig. 6a, at $T = 0$, the average displacement $u_{\theta,ave.T}^{P(0)\sim P(2\pi)}(\varphi) \neq 0$, which means under free rolling, the slippage may happen as discussed in the previous paper [14].

Figure 6b shows the effect of T/T_m on the displacement increase rate $\mathrm{d}u_{\theta}^{P(0)\sim P(2\pi)}(\theta,\varphi)/\mathrm{d}\varphi$ at the initial one roll rotation $\varphi = 2\pi$ when the load $P = P_0$ for the elastic shaft E_{shaft} = 210 GPa as well as rigid shaft $E_{shaft} = \infty$. With increasing T/T_m, $\mathrm{d}u_{\theta}^{P(0)\sim P(2\pi)}(\theta,\varphi)/\mathrm{d}\varphi$

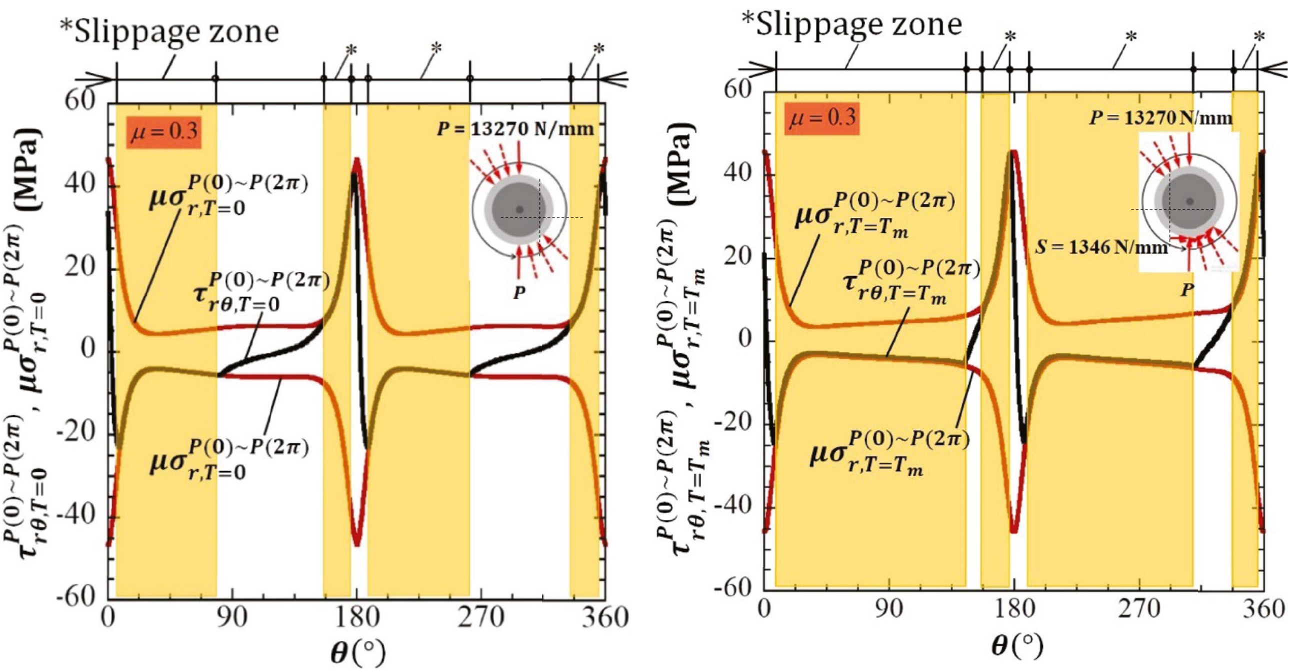

(a) Elastic shaft E_{shaft} = 210 GPa after the initial one roll rotation P P π with $T = 0$.

(b) Elastic shaft E_{shaft}=210 GPa after the initial one roll rotation $P(0)\sim P(2\pi)$ with T T_m.

Fig. 5 Comparison of the slippage zone where $\tau_{r\theta} \cong |\mu\sigma_r|$ for **a** the elastic shaft $E_{\text{shaft}} = 210$ GPa with $T = 0$ and **b** the elastic shaft $E_{\text{shaft}} = 210$ GPa with $T = T_m$, both under the loading shift $P(0) \sim P(2\pi)$ and $\mu = 0.3$

increases significantly. The displacement increase rate $\mathrm{d}u_\theta^{P(0)\sim P(2\pi)}(\theta,\varphi)/\mathrm{d}\varphi$ under the rated motor torque $T = T_m$ for the elastic shaft is 5 times larger than the one of the rigid shaft, and $\mathrm{d}u_\theta^{P(0)\sim P(2\pi)}(\theta,\varphi)/\mathrm{d}\varphi$ under $T = 3T_m$ for the elastic shaft is 19 times larger than the one of the rigid shaft. In the early stage of our study, we assumed the rigid shaft modeling by focusing on the sleeve displacement. However, Fig. 6a, b show the elastic shaft modeling is necessary. In Figs. 4b and 6b, at $T = 0$, the displacement increase rate $\mathrm{d}u_\theta^{P(0)\sim P(2\pi)}(\theta,\varphi)/\mathrm{d}\varphi \neq 0$, which may cause the slippage under free rolling $T = 0$ [14].

Next, in addition to the no torque condition $T = 0$ and the standard rolling conditions $P = P_0, T = T_m$, the extreme condition $P = 3P_0, T = 3T_m$ is considered. Here $P = 3P_0, T = 3T_m$ is assumed to be in the state of rolling trouble. In Fig. 6c, the solid line shows the effect of T/T_m on the average displacement $u_{\theta,ave.T}^{P(0)\sim P(2\pi)}(\varphi)$ when both P and T increase proportionally. The average displacement $u_{\theta,ave.T}^{P(0)\sim P(2\pi)}(\varphi)$ for the elastic shaft $E_{shaft} = 210$ GPa under $P = 3P_0, T = 3T_m$ is 20 times larger than that of $P = P_0, T = T_m$. In addition, under the rolling trouble state $P = 3P_0, T = 3T_m$ and $u_{\theta,ave.T}^{P(0)\sim P(2\pi)}(\varphi)$ for the elastic shaft is 8 times larger than that of the rigid shaft. In Fig. 6c, the dotted line shows the average displacement $u_{\theta,ave.T}^{P(0)\sim P(2\pi)}(\varphi)$ when the load P is fixed as $P = P_0, P = 2P_0$ and $P = 3P_0$ by varying the motor torque T. Under fixed $P = P_0$, the average displacement $u_{\theta,ave.T}^{P(0)\sim P(2\pi)}(\varphi)$ at $T = 3T_m$ is 5 times larger than $u_{\theta,ave.T}^{P(0)\sim P(2\pi)}(\varphi)$ at $T = T_m$. However, under fixed $T = T_m$, the average displacement $u_{\theta,ave.T}^{P(0)\sim P(2\pi)}(\varphi)$ at $P = 3P_0$ is 10 times larger than that at $P = P_0$. This observation explained that the effect P on the average displacement $u_{\theta,ave.T}^{P(0)\sim P(2\pi)}(\varphi)$ is larger than the effect T.

In Fig. 5d, the solid line shows the effect of T/T_m on the increase rate of interfacial displacement $\mathrm{d}u_\theta^{P(0)\sim P(2\pi)}(\theta,\varphi)/\mathrm{d}\varphi$ when P and T increase proportionally. The displacement increase rate $\mathrm{d}u_\theta^{P(0)\sim P(2\pi)}(\theta,\varphi)/\mathrm{d}\varphi$ for elastic shaft $E_{shaft} = 210$ GPa under $P = 3P_0, T = 3T_m$ is 70 times larger than that of $P = P_0, T = T_m$. In addition, under the rolling trouble state $P = 3P_0, T = 3T_m$ and $\mathrm{d}u_\theta^{P(0)\sim P(2\pi)}(\theta,\varphi)/\mathrm{d}\varphi$ for the elastic shaft is 31 times larger than that of the rigid shaft. In Fig. 5d, the dotted line shows the displacement increase rate $\mathrm{d}u_\theta^{P(0)\sim P(2\pi)}(\theta,\varphi)/\mathrm{d}\varphi$ when the load P is fixed as $P = P_0, P = 2P_0$ and $P = 3P_0$ by varying the motor torque T. Under fixed $P = P_0$, the displacement increase rate $\mathrm{d}u_\theta^{P(0)\sim P(2\pi)}(\theta,\varphi)/\mathrm{d}\varphi$ at $T = 3T_m$ is 10 times larger than $\mathrm{d}u_\theta^{P(0)\sim P(2\pi)}(\theta,\varphi)/\mathrm{d}\varphi$ at $T = T_m$. However, under fixed $T = T_m$, the displacement increase rate $\mathrm{d}u_\theta^{P(0)\sim P(2\pi)}(\theta,\varphi)/\mathrm{d}\varphi$

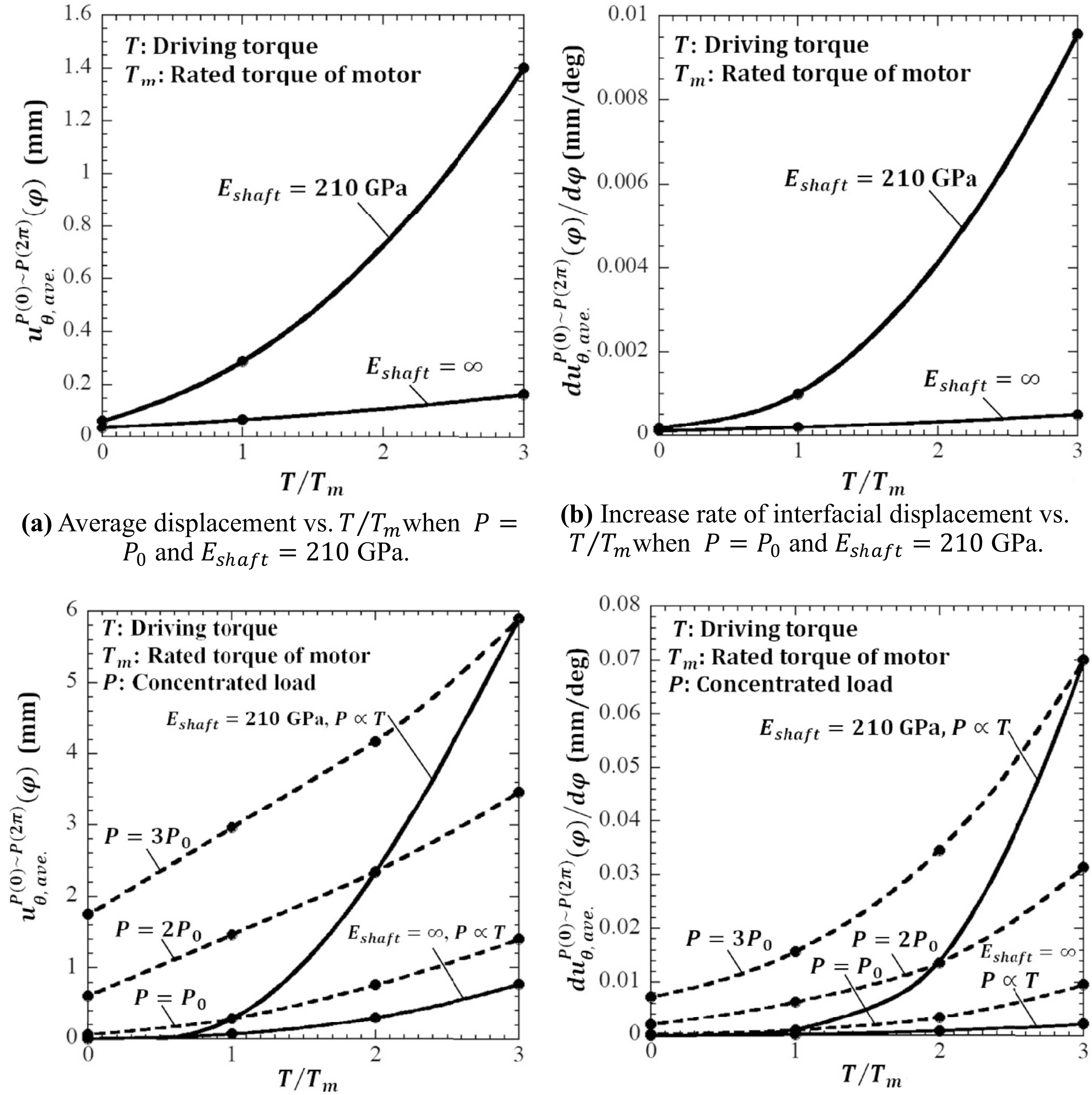

(a) Average displacement vs. T/T_m when $P = P_0$ and $E_{shaft} = 210$ GPa.

(b) Increase rate of interfacial displacement vs. T/T_m when $P = P_0$ and $E_{shaft} = 210$ GPa.

(c) Average displacement vs. T/T_m for $E_{shaft} = 210$ GPa when $P = P_0$, $P = 2P_0$ and $P = 3P_0$.

(d) Increase rate of interfacial displacement vs. T/T_m for $E_{shaft} = 210$ GPa when $P = P_0$, $P = 2P_0$ and $P = 3P_0$.

Fig. 6 Average displacement and increase rate of displacement vs. T/T_m when $\varphi = 2\pi$

at $P = 3P_0$ is 16 times larger than that at $P = P_0$. The larger change can be seen in the displacement increase rate $\mathrm{d}u_{\theta}^{P(0)\sim P(2\pi)}(\theta, \varphi)/\mathrm{d}\varphi$ compared to the average displacement $u_{\theta,ave.T}^{P(0)\sim P(2\pi)}(\varphi)$. If the rolling trouble happens, care should be taken for $\mathrm{d}u_{\theta}^{P(0)\sim P(2\pi)}(\theta, \varphi)/\mathrm{d}\varphi$ increases abruptly.

As shown in Fig. 6c, d, under zero torque $T = 0$, the average displacement $u_{\theta,ave.T}^{P(0)\sim P(2\pi)}(\varphi)$ as well as the displacement increase rate $\mathrm{d}u_\theta^{P(0)\sim P(2\pi)}(\theta,\varphi)/\mathrm{d}\varphi$ increases with increasing the loading force P. Therefore, the circumferential slippage under free rolling can be explained from the non-uniform deformation due to the rolling force P. In this way, the reason why there is still resultant circumferential slip in the case of zero torque [14] becomes clearer in this paper.

4.2 Effect of shrink fit ratio δ/d on non-uniform slip

To prevent the overall sleeve slippage in shrink-fitted rolling roll, the slip resistance torque T_r in Eq. 1 should be larger than the motor torque as $T_r > T$, but also the non-uniform slip considered in this study may happen. In this section, the shrink-fitting ratio controlling the shrink-fitting pressure $\sigma_{r_{shrink}}$ in Eq. (1) is focused. In the above discussion, the shrink-fitting ratio $\delta/d = 0.5\times10^{-3}$ is fixed to clarify the effect of the motor torque T on the interface slippage. When $\delta/d = 0.5\times10^{-3}$, the slip resistance torque T_r is larger than the rated motor toque T_m as $T_r = 6.77T_m$. Generally, in the sleeve assembly type roll, the shrink-fitting ratio is applied in the range $\delta/d = 0.4\times10^{-3} \sim 1.0\times10^{-3}$. The limitation of δ/d range is based on many years of experience. This is because a smaller value $\delta/d < 0.4\times10^{-3}$ may cause an interface to slip easily and a larger value $\delta/d > 1.0\times10^{-3}$ may increase the risk of sleeve fracture [6].

Figure 7 indicates the increase rate of interfacial displacement $\mathrm{d}u_\theta^{P(0)\sim P(2\pi)}(\theta,\varphi)/\mathrm{d}\varphi$ by varying the shrink-fitting ratio δ/d in the range $\delta/d = 0 \sim 1.0\times10^{-3}$. The displacement increase rate $\mathrm{d}u_\theta^{P(0)\sim P(2\pi)}(\theta,\varphi)/\mathrm{d}\varphi$ decreases with increasing shrink-fitting ratio δ/d regardless of the torque condition. This is because with increasing δ/d, the fitting pressure $\sigma_{r_{shrink}}$ increases. Then the slip resistance increases and the displacement increasing rate $u_\theta^{P(0)\sim P(2\pi)}(\theta,\varphi)/\mathrm{d}\varphi$ decrease.

When the shrink-fitting ratio $\delta/d = 0$, the displacement increase rate $du_\theta^{P(0)\sim P(2\pi)}(\theta,\varphi)/d\varphi$ is not infinite because the roll is pressed by a pair of loads P which generate the contact pressure at the interface and causing the slip resistance at the contact portion. On the other hand, when $\delta/d \to \infty$, the sleeve and the shaft are integrated together without slippage and therefore $du_\theta^{P(0)\sim P(2\pi)}(\theta,\varphi)/d\varphi \to 0$.

In addition, under the reference value $\delta/d = 0.5\times10^{-3}$, the displacement increasing rate $\mathrm{d}u_\theta^{P(0)\sim P(2\pi)}(\theta,\varphi)/\mathrm{d}\varphi = 7.0\times10^{-2}$ mm/deg when $T = 3T_m, P = 3P_0$ which is about 70 times larger than $\mathrm{d}u_\theta^{P(0)\sim P(2\pi)}(\theta,\varphi)/\mathrm{d}\varphi = 0.1\times10^{-2}$ mm/deg when $T = T_m, P = P_0$. To prevent inner fracture of the sleeve, by using large δ/d, care should be taken for the large circumferential stress σ_θ appearing at the inner surface causing the fracture.

4.3 Effect of friction coefficient μ on non-uniform slip

The friction coefficient is the main factor as well as the shrink-fitting ratio to prevent interfacial slip. Therefore, in this section, the friction coefficient is changed in the range $\mu = 0.1 \sim 1.0$ including the reference value $\mu = 0.3$. In the expimental study, $\mu = 0.2$ was used between the sleeve inner surface and the shaft outer surface [1]. In addition, $\mu = 0.4$ was reported as a friction coefficient between steels [38]. In this way, the values around $\mu = 0.2 \sim 0.4$ are often used on the sleeve roll joint surface. It is known that among many metals used in steel industries, pure metals have a higher friction coefficient than other alloys. Therefore, the friction coefficient μ should be considered in combination with Armco iron, which can be regarded to be very close to pure iron [40]. Then, the highest friction coefficient can be $\mu = 0.82$ for Armco iron/aluminum combination, $\mu = 0.58$ for Armco iron/nickel, and $\mu = 0.52$ for Armco iron/iron. Therefore, in this study, $\mu = 1.0$ is used as the upper limit of the friction coefficient in a practical sense.

Figure 8 shows the displacement increase rate $\mathrm{d}u_\theta^{P(0)\sim P(2\pi)}(\theta,\varphi)/\mathrm{d}\varphi$ by varying the friction coefficient μ. It can be seen that the displacement increase rate $\mathrm{d}u_\theta^{P(0)\sim P(2\pi)}(\theta,\varphi)/\mathrm{d}\varphi$ decreases with increasing friction coefficient μ regardless of the torque condition. Large shrink-fitting ratio δ/d and large friction coefficient μ can be used to prevent interfacial slippage, although there is a restriction on the range of use. Although large δ/d and large μ may prevent the interfacial slippage, it is difficult to use such δ/d and μ under the rolling trouble $T = 3T_m, P = 3P_0$.

4.4 Conventional design concept versus new design concept for sleeve roll

Finally, Fig. 9 summarizes the difference between the conventional design concept and the new design concept

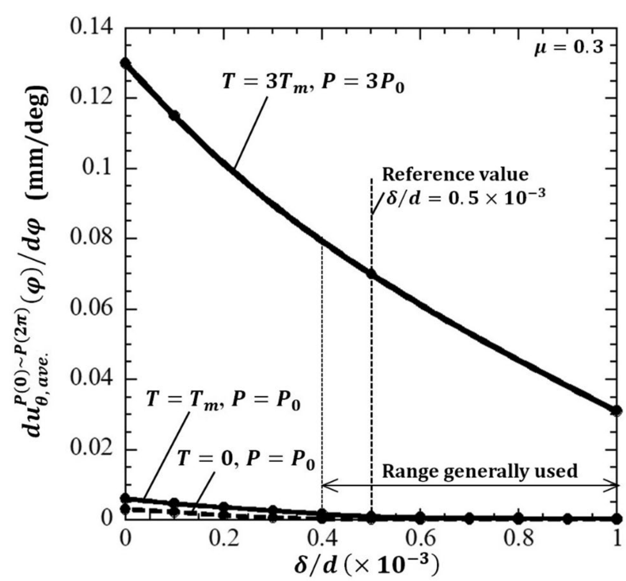

Fig. 7 Increase rate of interfacial displacement vs. δ/d when $\varphi = 2\pi$, $T = 0, P = P_0, T = T_m, P = P_0$, and $T = 3T_m, P = 3P_0$

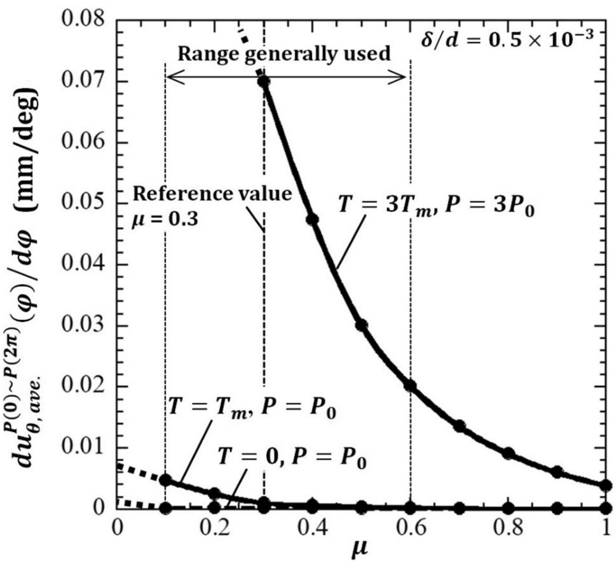

Fig. 8 Increase rate of interfacial displacement vs friction coefficient μ when $\varphi = 2\pi$, $T = 0, P = P_0$, $T = T_m, P = P_0$, and $T = 3T_m, P = 3P_0$

obtained from the discussion of this paper. As shown in Fig. 9a, the conventional method prescribes $T < T_r$ from Eq. (1). Instead, the new method prescribes that the small amount of the interfacial slip may occur even under $T < T_m$. Therefore, based on Fig. 9b, a proper key should be designed to prevent interfacial slip.

5 Conclusions

The shrink-fitted sleeve roll has several advantages. For example, the sleeve wear resistance can be improved independently without loosening the shaft ductility. In addition, the shaft can be reused by replacing the damaged sleeve. In this paper, the FEM simulation was performed to clarify the interfacial slip in real rolling by varying the motor driving torque. To clarify the phenomena, the increase rate of the interfacial displacement was mainly focused. The effects of the shrink-fitting ratio and the effect of the friction coefficient were also considered. The conclusions can be summarized in the following way:

1. The displacement increase rate gradually increases during the initial one rotation and becomes constant after the initial rotation regardless of the amount of motor torque T. In other words, the interfacial slip is unstable during the initial one rotation but becomes stable after that. Therefore, the amount of the interfacial slip can be predicted from the displacement increase rate because the phenomenon becomes stable after one rotation (see Fig. 4).
2. Under the rated motor torque $T = T_m$, the displacement increase rate is about five times larger than the rate under free rolling $T = 0$ (see Fig. 4). The acceleration effect of the motor torque T can be explained by the "slippage zone" where the frictional stress and shear stress are equal. The slip zone becomes larger under the rated motor torque $T = T_m$ compared to the one under free rolling $T = 0$ (see Fig. 5).
3. With increasing the motor torque T as well as the loading force as $P \propto T$, the displacement increase rate increases significantly (see Fig. 6). Under the load conditions $T = 3T_m$ and $P = 3P_0$ corresponding to the rolling trouble, the increase rate is 70 times larger than under the standard rolling condition $T = T_m$ and $P = P_0$ (see Fig. 6).
4. The circumferential slippage under free rolling can be explained from the non-uniform deformation due to the loading force P. This is because the displacement increase rate under zero torque increases with increasing the loading force P (see Fig. 6c).
5. With increasing the shrink fit rate δ/d, the displacement increase rate decreases significantly (see Fig. 7). With increasing the friction coefficient μ, the displacement increase rate decreases significantly (see Fig. 8). The effect of the motor torque on the elastic shaft is much larger compared to the rigid shaft (see Fig. 6a, b).
6. Since the conventional design concept is based on the total slip, a novel design concept based on the non-uniform slip was proposed (see Fig. 9a, b).

Appendix. Experimental confirmation for interfacial slip by using miniature roll under free rolling

In this paper, the effect of the motor torque on the interfacial slip is mainly investigated through numerical simulation. To verify the simulation experimentally, Fig. 10 illustrates the miniature roll specimen whose diameter is 60 mm used to confirm the interfacial slip [14]. Table 2 shows the experimental conditions with no motor torque because a similar phenomenon known as "interfacial creep" in ball bearing was under free rolling. The work roll consists of two sleeves and a shaft. To realize the slip between sleeve 1 and sleeve 2 in Fig. 10 sleeve 2 and the inserted shaft are fixed by the key. In the experiment, the work roll was cooled down by water at room temperature to prevent the change of the shrink-fitting ratio due to rising temperature. Under the steady rotation, the load of 1 ton was applied confirming the roll surface temperature change was within 5 °C or less during the experiment by a contact thermometer.

The FEM simulation is also performed by using the mesh in Fig. 10. Four-node quadrilateral plane strain elements are used, and the total number of mesh elements is 7408.

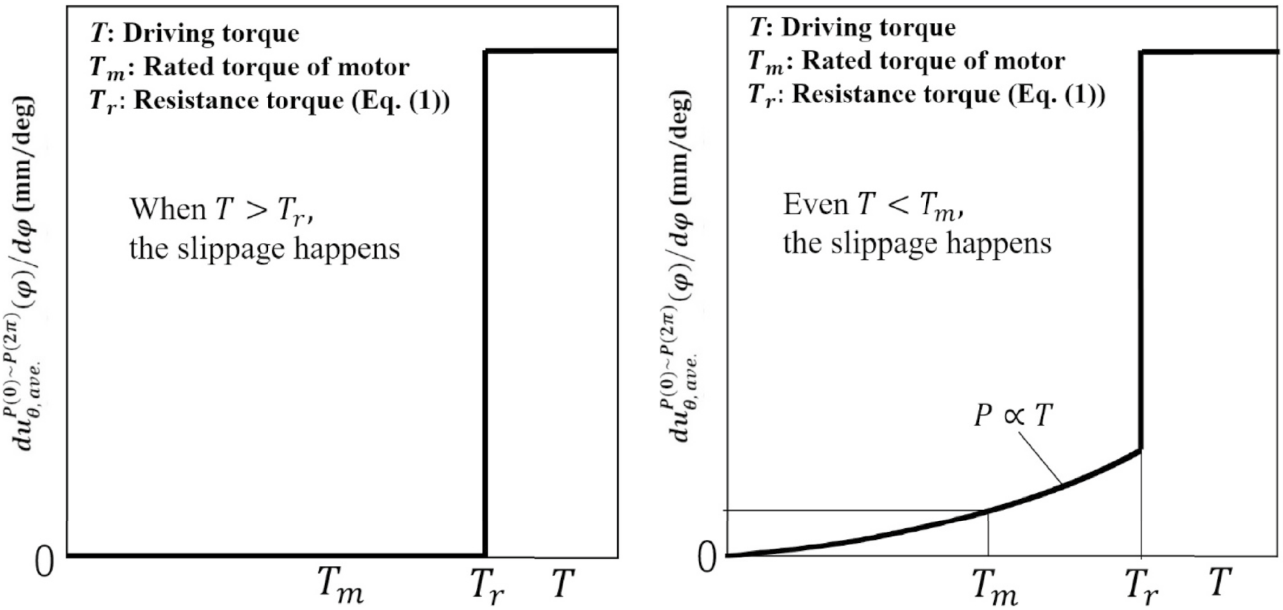

(a) Conventional design concept based on overall slip in sleeve roll.

(b) New design concept based on non-uniform slip in sleeve roll.

Fig. 9 Conventional design concept versus new design concept for sleeve roll

Table 2 Experimental conditions by using a miniature roll in Fig. 10

Test roll	
Shrink-fitting ratio $\delta/d = 0.21 \times 10^{-3}$	
Driving condition	
Test roll	Free rolling
Pair roll	Driven by the torque 457Nm
Load P (ton)	1.0
Rotating speed (rpm)	106 ~ 212
Roll cooling: front side (L/min), back side	Water 0.25, 2.0
	16.0 ~ 21.0
Roll temperature (℃): $\delta/d = 0.21 \times 10^{-3}$, 0	Rotations until sleeve slip
Number of rotation n	

Table 3 Comparison of experimental data and simulation results for average displacement during one roll rotation

	Shrink-fitting ratio $\delta/d = 0.21 \times 10^{-3}$		
	Experimental results for miniature roll in Fig. 10	Simulation results for miniature roll in Fig. 10	Simulation results for real roll in Fig. 1
$u_{\theta,ave.}^{P(0)\sim P(2\pi)}$	0.108×10^{-2} mm	0.384×10^{-2} mm	2.92×10^{-2} mm

Fig. 10 FEM mesh for test specimen used in a miniature roll

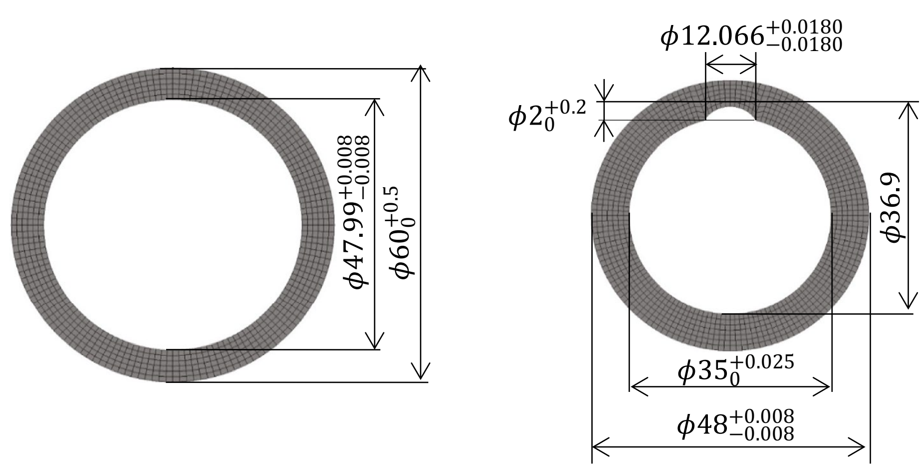

(a) Sleeve 1

(b) Sleeve 2

By assuming the loading $P = 245$ N/mm, the shrink-fitting ratio $\delta/d = 0.21 \times 10^{-3}$ and the constant friction coefficient $\mu = 0.3$ between sleeve 1 and sleeve 2, the numerical simulation is newly performed for the miniature roll. Similar to Fig. 3b, $u_\theta^{P(0)\sim P(\varphi)}(\theta)$ is defined as the relative displacement between sleeve 1 and sleeve 2. Table 3 summarizes the average values of the displacement obtained by the simulation in comparison with the slip distance in the experiment when $\delta/d = 0.21 \times 10^{-3}$. The experimental value corresponds to $u_{\theta,ave.}^{P(0)\sim P(2\pi)}$ during one roll rotation that can be calculated in the following way:

$$\begin{aligned} u_{\theta,ave.}^{P(0)\sim P(2\pi)} &= \frac{\theta_{\text{slip}} \times \pi d}{360^\circ \times n} \\ &= \frac{77^\circ \times \pi \times 48mm}{360^\circ \times 3 \times 10^4} \\ &= \frac{32mm}{3 \times 10^4} \\ &= 0.108 \times 10^{-2} mm \end{aligned} \tag{7}$$

In Eq. (7), θ_{slip} is the slip angle observed in the experiment, d is the inner diameter of sleeve 1 and n is the number of the roll rotation.

As shown in Table 3, although the numerical simulation result is 3.56 times larger than the experimental result, their orders are in agreement. The difference can be explained by the experimental observation. Due to the circumferential slip, slip defects start with thin and shallow scratches, then, it becomes thicker and deeper with erosive wear and cohesive wear, and eventually form large defects that completely stop the slip. In the simulation, a constant friction coefficient $\mu = 0.3$ should be changed to $\mu = 0.3 \sim \infty$, but actually the change reflecting the real defect evolution is almost impossible in practice. This is the reason why 3.56 times difference appears between the experiment and the simulation. Although the experimental and simulation results are not in good agreement, the model is useful for understanding the phenomenon especially when this is no slip defect, and the model can be used for comparative purposes or similar claims.

Availability of data and material The data presented in this study are available on request.

Declarations

Ethics approval Not applicable.

Consent to participate Not applicable.

Consent for publication Not applicable.

Conflict of interest The authors declare no competing interests.

References

1. Shimoda H, Onodera S, Hori K (1966) Study on the residual deflection of large sleeved back-up rolls: 4th Report, Residual stresses of sleeved rolls. Trans Jpn Soc Mech Eng 32:689–694
2. Tutumi S, Hara S, Yoshi S (1971) The residual deflection of sleeved backup-up rolls. Tetsu Hagane 57(5):818–822
3. Noda NA, Sano Y, Takase Y, Shimoda Y, Zhang G (2017) Residual deflection mechanism for back-up roll consisting of shrink-fitted sleeve and arbor. J JSTP 58:66
4. Irie T, Takaki K, Tsutsunaga I, Sano Y (1979) Steel strip and section steel and thick rolling, processing. Tetsu Hagane 65:293
5. Takigawa H, Hashimoto K, Konno G, Uchida S (2003) Development of forged high-speed-steel roll for shaped steel. CAMP-ISIJ 16:1150–1153
6. Sano Y (1993) Recent advances in rolling rolls. Proc of the No. 148–149 Nishiyama Memorial Technology Course, Tokyo, Japan, 193–226
7. Sano Y (1999) Fatigue failure problem in the inside of roll body for hot strip rolling- crack initiation problem and its estimation in the actual plant. The 245th JSMS Committee on Fatigue of Materials and The 36th JSMS Committee on Strength Design, Safety Evaluation 40
8. Matsunaga E, Tsuyuki T, Sano Y (1998) Optimum shrink fitting ratio of sleeve roll (Strength design of shrink fitted sleeve roll for hot strip mill-1). CAMP-ISIJ 11:362. https://ci.nii.ac.jp/naid/10002551803
9. Spuzic S, Strafford KN, Subramanian C, Savage G (1994) Wear of hot rolling mill rolls: an overview. Wear 176(2):261–271. https://doi.org/10.1016/0043-1648(94)90155-4
10. Noda NA, Hu K, Sano Y, Ono K, Hosokawa Y (2016) Residual stress simulation for hot strip bimetallic roll during quenching. Steel Res Int 87(11):1478–1488. https://doi.org/10.1002/srin.201500430
11. Hu K, Xia Y, Zhu F, Noda NA (2017) Evaluation of thermal breakage in bimetallic work roll considering heat treated residual stress combined with thermal stress during hot rolling. Steel Res Int 89(4):1700368. https://doi.org/10.1002/srin.201700368
12. Noda NA, Sakai H, Sano Y, Takase Y, Shimoda Y (2018) Quasi-equilibrium stress zone with residual displacement causing permanent slippage in shrink-fitted sleeve rolls. Metals 8(12):998. https://doi.org/10.3390/met8120998
13. Sakai H, Noda NA, Sano Y, Zhang G, Takase Y (2019) Numerical simulation on interfacial creep generation for shrink-fitted bimetallic roll. ISIJ Int 59(5):889–894. https://doi.org/10.2355/isijinternational.ISIJINT-2018-749
14. Noda NA, Rafar RA, Sakai H, Zheng X, Tsurumaru H, Sano Y, Takase Y (2021) Irreversible interfacial slip in shrink-fitted bimetallic work roll promoted by roll deformation. Eng Fail Anal 126:105465. https://doi.org/10.1016/j.engfailanal.2021.105465
15. Noda NA, Rafar RA, Sano Y (2021) Stress due to interfacial slip causing sleeve fracture in shrink-fitted work roll. Int J Modern Phys B 2140020. https://doi.org/10.1142/S0217979221400208
16. Soda N (1964) Bearing. Iwanami Shoten, Tokyo, pp 196–203
17. Imai M (1959) Creep of the roller bearing. Lubrication: Journal of Japan Society of Lubrication Engineers 4(6):307–312
18. Murata J, Onizuka T (2005) Generation mechanism of inner ring creep. Koyo Eng J 166:41–47
19. Niwa T (2013) A creep mechanism of rolling bearings. NTN Tech Rev 81:100–103
20. Ten S, Takemura Y (2006) NSK Tech J 680:13
21. NSK (1997) New bearing doctor: diagnosis of bearing problems. Objective: Smooth & Reliable Operation. https://www.nsk.com/common/data/ctrgPdf/e7005c.pdf

22. Zhan J, Takemura H, Yukawa K (2007) A study on bearing creep mechanism with FEM simulation. Proceedings of IMECE2007, 2007 Seattle, Washington, USA. https://doi.org/10.1115/IMECE2007-41366
23. Zhan J, Yukawa K, Takemura H (2009) Analysis of bearing outer ring creep with FEM. Advanced Tribology, 2009, Springer Berlin, Heidelberg. https://doi.org/10.1007/978-3-642-03653-8_74
24. Noguchi S, Ichikawa K (2010) A study about creep between inner ring of ball bearing and shaft. Proc Acad Lect Japan Soc Precis Eng. https://doi.org/10.11522/pscjspe.2010A.0.565.0
25. Teramoto T, Sato Y (2015) Prediction method of outer ring creep phenomenon of ball bearing under bearing load. Trans Soc Autom Eng Japan 46:355–360. https://doi.org/10.11351/jsaeronbun.46.355
26. Bovet C, Zamponi L (2016) An approach for predicting the internal behaviour of ball bearings under high moment load. Mech Mach Theory 101:1–22. https://doi.org/10.1016/j.mechmachtheory.2016.03.002
27. Miyazaki T, Noda NA, Ren F, Wang Z, Sano Y, Iida K (2017) Analysis of intensity of singular stress field for bonded cylinder and bonded pipe in comparison with bonded plate. Int J Adhes Adhes 77:118–137. https://doi.org/10.1016/j.ijadhadh.2017.03.019
28. Noda NA, Miyazaki T, Li R, Uchikoba T, Sano Y, Takase Y (2015) Debonding strength evaluation in terms of the intensity of singular stress at the interface corner with and without fictitious crack. Int J Adhes Adhes 61:46–64. https://doi.org/10.1016/j.ijadhadh.2015.04.005
29. Noda NA, Uchikoba T, Ueno M, Sano Y, Iida K, Wang Z, Wang G (2015) Convenient debonding strength evaluation for spray coating based on intensity of singular stress. ISIJ Int 55(12):2624–2630. https://doi.org/10.2355/isijinternational.ISIJINT-2015-458
30. Wang Z, Noda NA, Ueno M, Sano Y (2016) Optimum design of ceramic spray coating evaluated in terms of intensity of singular stress field. Steel Res Int 88:1–9. https://doi.org/10.1002/srin.201600353
31. Noda NA, Chen X, Sano Y, Wahab MA, Maruyama H, Fujisawa R, Takase Y (2016) Effect of pitch difference between the bolt-nut connections upon the anti-loosening performance and fatigue life. Mater Des 96:476–489. https://doi.org/10.1016/j.matdes.2016.01.128
32. Noda NA, Takaki R, Shen Y, Inoue A, Sano Y, Akagi D, Takase Y, Galvez P (2019) Strain rate concentration factor for flat notched specimen to predict impact strength for polymeric materials. Mech Mater 131:141–157. https://doi.org/10.1016/j.mechmat.2019.01.011
33. Matsuda S, Suryadi D, Noda NA, Sano Y, Takase Y, Harada S (2013) Structural design for ceramics rollers used in the heating furnace. Trans JSME Ser A 79(803):989–999
34. Noda NA, Suryadi D, Kumasaki S, Sano Y, Takase Y (2015) Failure analysis for coming out of shaft from shrink-fitted ceramics sleeve. Eng Fail Anal 57:219–235. https://doi.org/10.1016/j.engfailanal.2015.07.016
35. Noda NA, Xu Y, Suryadi D, Sano Y, Takase Y (2016) Coming out mechanism of steel shaft from ceramic sleeve. ISIJ Int 56(2):303–310. https://doi.org/10.2355/isijinternational.ISIJINT-2015-558
36. Zhang G, Sakai H, Noda NA, Sano Y, Oshiro S (2019) Generation mechanism of driving out force of the shaft from the shrink fitted ceramic roll by introducing newly designed stopper. ISIJ Int 59(2):293–299. https://doi.org/10.2355/isijinternational.ISIJINT-2018-615
37. Marc Mentat Team (2008) Theory and user information, Vol. A, MSC, Software, Tokyo, 713
38. Misumi-vona Top, Technical information, Dry coefficient of friction. https://jp.misumi-ec.com/tech-info/categories/plastic_mold_design/pl07/c0874.html Accessed 20 Jul 2020
39. Hot Strip Subcommittee of Joint Study Group of Steel Sheet Subcommittee in The Iron and Steel Institute of Japan: Recent hot strip manufacturing technology in Japan (Report of Hot Strip Subcommittee of Joint Study Group of Steel Sheet Subcommittee), Ibaraki Print (1987), 255
40. JSME (2004) Mechanical Engineering Handbook a2 Mechanical Mechanics, JSME, pp 27

Publisher's note Springer Nature remains neutral with regard to jurisdictional claims in published maps and institutional affiliations.